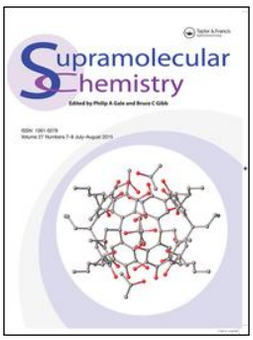

Supramolecular Chemistry

ISSN: (Print) (Online) Journal homepage: https://www.tandfonline.com/loi/gsch20

Substitution effects on the binding interactions of redox-active arylazothioformamide ligands and copper(I) salts

Rabina Pradhan , Vincent M. Groner , Kaylaa L. Gutman , Zachariah M. Heiden , Mark F. Roll , James G. Moberly & Kristopher V. Waynant

To cite this article: Rabina Pradhan , Vincent M. Groner , Kaylaa L. Gutman , Zachariah M. Heiden , Mark F. Roll , James G. Moberly & Kristopher V. Waynant (2020): Substitution effects on the binding interactions of redox-active arylazothioformamide ligands and copper(I) salts, Supramolecular Chemistry, DOI: 10.1080/10610278.2020.1795172

To link to this article: https://doi.org/10.1080/10610278.2020.1795172

Published online: 30 Jul 2020.

SUPRAMOLECULAR CHEMISTRY
https://doi.org/10.1080/10610278.2020.1795172

Taylor & Francis
Taylor & Francis Group

ARTICLE

Substitution effects on the binding interactions of redox-active arylazothioformamide ligands and copper(I) salts

Rabina Pradhan[a], Vincent M. Groner[a], Kaylaa L. Gutman[a], Zachariah M. Heiden[b], Mark F. Roll[c], James G. Moberly[c] and Kristopher V. Waynant[a]

[a]Dept. Of Chemistry, University of Idaho, Moscow, USA; [b]Dept. Of Chemistry, Washington State University, Pullman, USA; [c]Dept. Of Chemical and Materials Engineering, University of Idaho, Moscow, USA

ABSTRACT

The straightforward synthesis of redox-active arylazothioformamide (ATF) ligands allows for electronic diversity as to measure the weak-binding interactions of transition metal salts in supramolecular coordination complexes. A small library of para-substituted ATFs was created with varied electronic components to evaluate how electron-donating and electron-withdrawing groups alter binding association constants. Following full characterisation, including single-crystal X-ray diffraction, UV-Vis titration studies were performed using copper(I) salts to assess the Host:Guest binding. Simultaneously, substitutions were evaluated computationally by modelling the Gibbs' Free Energy change of the rotational barriers from ligand crystal structures to the predicted metal coordinating species and the various complexes. The multi-model association calculations and experimental measurements interplay to help limit error propagations and reliably predict the more accurate binding models. Through a thorough investigation it was found that experimentally, each ligand supports a 2:1 binding model yet may employ unique binding mechanisms to achieve that model.

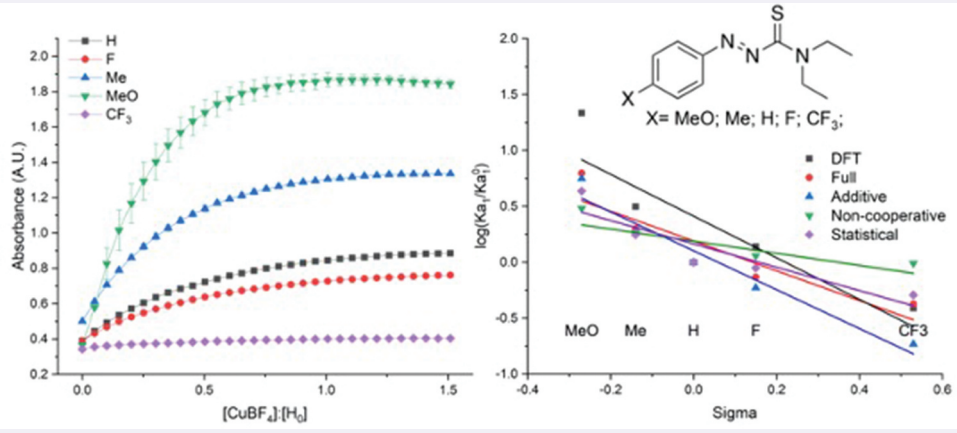

ARTICLE HISTORY
Received 4 February 2020
Accepted 30 June 2020

KEYWORDS
Host:guest; arylazothioformamide; substitution effects

Introduction

Redox-active arylazothioformamide (ATF) coordination complexes with late transition metals were first reported in the late 1970s [1,2] and then again in the early 2000s for use as material purification agents [3–5]. ATF has been shown to bind through the 1,4-azothiocarbonyl heterodiene moiety to various zero-valent late transition metals (Cu, Pd, Pt, Ni) resulting in redox activity and significant increases (4,000 to 8,000 fold) in molar extinction coefficients, thus allowing for detection of low levels of the metal:ligand complex by UV-Vis spectroscopy.

With a simple structure, as shown in Scheme 1, the non-substituted ATF ligand **1** has been shown to crystallise with Cu(I) salts in non-redox active 1:1 (**2**) μ-halide dimers and 2:1 (**3**) arrangements, depending on the counter anion [6]. By modifying the electronics of the system, the redox-activity and binding association of the ligand may be affected, altering association constants, and potentially inducing redox activity. X-ray crystal structures of the metal:ligand coordination complexes of **1** with the various Cu(I) salts serve as starting points for computational modelling of both the rotation of the 1,4 azothiocarbonyl heterodiene into binding coordination and of the energy

CONTACT Kristopher V. Waynant kwaynant@uidaho.edu Moscow, ID 83844

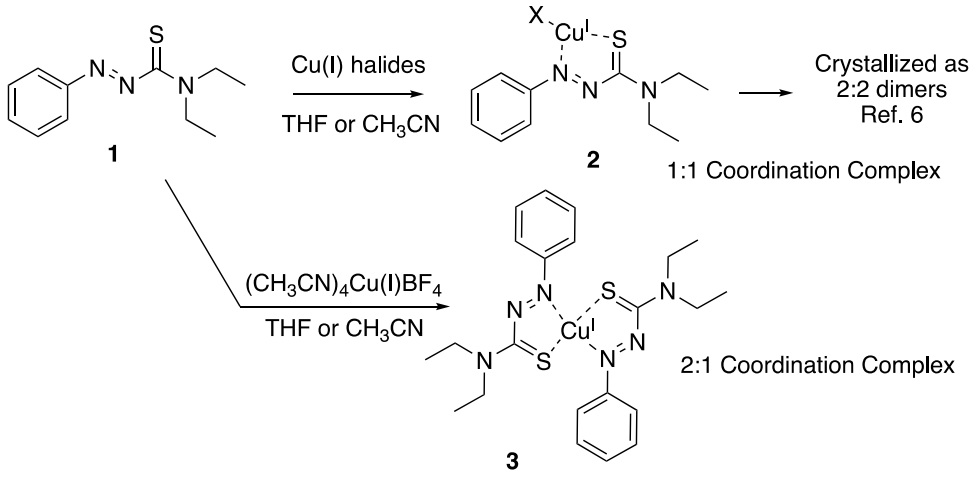

Scheme 1. Binding interactions seen with arylazothioformamide ligand 1 and various Cu(I) salts.

differences between the neutral and the singly reduced forms of the ligand[7]. Extending the information from crystallography, computational modelling provides predictions for H:G interactions and strengthening or weakening of chemical alterations prior to coordination. The simplicity of the ATF structure lends itself to both computational and synthetic substitution approaches. Herein, a small library of para-substituted ATF ligands, which range from strong electron donating to strong electron withdrawing, was prepared, crystallised, and evaluated to explore substitution effects on Cu(I) coordination. Crystal structures were adapted into computational models to predict Gibb's free energy changes and experimental UV-Vis titration studies were performed with various Cu(I) salts to validate binding association predictions. Both 1:1 and 2:1 binding models were assessed to compare to computational expectations. Our hypothesis is that the addition of electron-donating substituents in the para-position will increase binding association while electron-withdrawing moieties will decrease binding or induce an oxidation event of the transition metal. The null hypothesis would predict no correlation between electronic substituents and binding affinity.

Materials and methods

Experimental procedures

***N,N*-diethyl-2-phenyldiazothioformamide (1)**: Ethanol (75 mL) was placed in a 200 mL 3-neck round bottom flask and degassed with nitrogen for 0.5 h. Phenylhydrazine (3.95 mL, 0.04 mol) was added followed by a dropwise addition of carbon disulphide (2.76 mL, 0.045 mol) and the solution was stirred for 0.5 h in which a precipitate formed. Potassium hydroxide (2.7 g, 0.048 mol) dissolved in degassed ethanol (25 mL) was then quickly poured into the mixture and the mixture immediately dissolved and turned light orange. This solution was stirred for 0.5 h after which methyl iodide (2.8 mL, 0.045 mol) was added in one aliquot and the mixture that had turned cloudy turned from maroon to a light yellow. This solution was stirred for 1 h and then ethanol and carbon disulphide were removed via rotary evaporation. Diethylamine (40 mL) was then added and the mixture was stirred at reflux overnight (thiosemicarbazone by NMR) before the reflux column and heat were removed. Oxygen in the form of air was then bubbled into the solution at room temperature for 2–4 h. After concentrating onto silica, column chromatography using 9:1 hexane: ethyl acetate yielded 6.0 g of a dense red oil (68%). This oil was subjected to recrystallisation using 20:1 heptane: ethyl acetate to receive orange needles. Physical data matched that of previous reports [6,8].

***N,N*-diethyl-2-(4-methoxyphenyl)diazothioformamide (5a)**: 75 mL of ethanol was degassed under nitrogen flow in a flame-dried round bottom fitted with a magnetic stirrer for 1 h. 4-methoxyphenylhydrazine•HCl (30.00 mmol, 5.821 g) was added and allowed to dissolve forming a dark purple solution. Carbon disulphide (34.2 mmol, 2.06 mL) was added dropwise and allowed to stir for 0.5 h. Potassium hydroxide (2.36 g, 42.0 mmol) dissolved in degassed ethanol (25 mL) was then quickly poured into the mixture and stirred the solution was stirred for 0.5 h. Following, methyl iodide (33.60 mmol, 2.09 mL) was added in one aliquot. The solution was stirred for 1 h before concentrating with a rotary evaporator to produce an orange solid. The flask was then fitted with a reflux condenser and put under inert nitrogen flow. Diethylamine (40 mL) was added and the solution was refluxed for 48 h. The resulting dark red solution was then opened to the air, allowed to cool to RT, and continued to stir for 2 h. The solution was then washed with brine and extracted with ethyl acetate to afford a dark red oil. The

resulting red liquid was concentrated via rotary evaporator and purified using flash column chromatography 7:3 hexane: ethyl acetate forming 4.693 g (62%) of orange solid. The resulting solid was recrystallised with 7:3 hexane: ethyl acetate to form dark red crystal. ^{1} H NMR (300 MHz, Chloroform-d) δ 7.89 (d, J = 9.0 Hz, 2 H), 6.99 (d, J = 9.0 Hz, 2 H), 4.03 (q, J = 7.1 Hz, 2 H), 3.90 (s, 3 H), 3.55 (q, J = 7.2 Hz, 2 H), 1.40 (t, J = 7.1 Hz, 3 H), 1.18 (t, J = 7.2 Hz, 3 H). ^{13} C NMR (125 MHz, $CDCl_3$) δ 195.0 164.3, 147.0, 126.7, 115.3, 56.5, 48.8, 45.9, 14.6, 12.3. FTIR (cm^{-1}): 2974,1579, 1419, 1259,1145, 775. Elemental Analysis: C_{12} $H_{17}N_3OS$ (251.35) (Calculated) C, 57.74; H, 6.756; N, 16.42 (Found) C, 57.34; H, 6.82; N, 16.72; mp: 93 °C.

***N,N*-diethyl-2-(p-tolyl)diazothioformamide (5b)**: 50 mL of ethanol and *p*-methylphenylhydrazine HCl (25.90 mmol, 4.11 g) was added to a flame-dried round-bottom flask and allowed to degas for 1.5 h under nitrogen flow. While under nitrogen, carbon disulphide (29.53 mmol, 2.25 ml) was added dropwise and the solution was allowed to stir under ambient conditions for an additional 0.5 h. Potassium hydroxide (32.37 mmol, 1.82 g) dissolved in degassed ethanol (20 mL) was then added into the mixture dropwise in a single aliquot and allowed to stir under nitrogen for 0.5 h resulting in the formation of a thick off-white liquid. Methyl iodide (29.01 mmol, 1.8 ml) was then added to the solution and stirred under nitrogen for 1 h. The resulting liquid was then concentrated with a rotary evaporator to afford a white paste. The flask was then equipped with a reflux condenser and put under nitrogen flow. Diethylamine (35 mL) was added and the mixture was refluxed under nitrogen for 48 h. The solution was cooled to ambient temperatures then exposed to air and allowed to stir for 2 h. The resulting red liquid was concentrated via rotary evaporator and purified using flash column chromatography 4:1 hexane: ethyl acetate forming 4.32 g (77%) of orange solid. The resulting solid was subjected to recrystallisation from the slow evaporation of acetonitrile to afford diffracting crystals. ^{1} H NMR (300 MHz, Chloroform-d) δ 7.97 (d, *J* = 8.3 Hz, 2 H), 7.79 (d, *J* = 8.4 Hz, 2 H), 4.03 (q, *J* = 7.3 Hz, 2 H), 3.50 (q, *J* = 7.2 Hz, 2 H), 1.54 (s, 3 H), 1.42 (t, *J* = 7.1 Hz, 3 H), 1.20 (t, *J* = 7.2 Hz, 3 H). ^{13} C NMR (126 MHz, $CDCl_3$) δ 195.2 (C = S), 150.9, 144.5, 130.8, 124.5, 48.7, 45.9, 22.5, 14.6, 12.3. FTIR (cm^{-1}): 2931, 1512, 1431, 1078, 782, 702. Elemental Analysis: (calculated) C_{12} $H_{17}N_3S$ (235.35) C, 61.24; H, 7.28; N, 17.85; (found) C, 61.24; H, 7.28; N, 17.85; S, 13.62. mp: 84 °C.

***N,N*-diethyl-2-(4-fluorophenyl)diazothioformamide (5c)**: 50 mL of ethanol and *p*-fluorophenylhydrazine HCl (24.29 mmol, 3.95 g) was added to a flame-dried round-bottom flask equipped with a magnetic stirrer and allowed to degas for 1.5 h under nitrogen flow. While under nitrogen, carbon disulphide (27.69 mol, 2.65 ml) was added dropwise to the flask and the solution was allowed to stir under ambient conditions for 0.5 h. Potassium hydroxide (1.63 g, 29.02 mol) dissolved in degassed ethanol (20 mL) was then added and allowed to stir under nitrogen for 0.5 h. Methyl iodide (27.20 mmol, 1.7 ml) was then added to the solution and stirred under nitrogen for 1 h. The resulting liquid was then concentrated with a rotary evaporator to afford an off-white paste. The flask was then equipped with a reflux condenser and put under nitrogen flow upon 30 mL of diethylamine was then added and the mixture was heated to reflux under nitrogen for 48 h. The solution was cooled to ambient temperature, opened to air, and allowed to stir for 2 h. The resulting red liquid was concentrated via rotary evaporator and purified using flash column chromatography 4:1 hexane: ethyl acetate forming 4.16 g (72%) of red solid. The resulting solid was subjected to recrystallisation using slow evaporation of acetonitrile to afford diffracting dark red crystals. ^{1} H NMR (300 MHz, Chloroform-*d*) δ 7.91 (t, 2 H), 7.19 (t, 2 H), 4.03 (q, *J* = 7.1, 2 H), 3.51 (q, *J* = 7.2 2 H), 1.41 (t, *J* = 7.2 Hz, 3 H), 1.18 (t, *J* = 7.2 Hz, 3 H). ^{13} C NMR (75 MHz, $CDCl_3$) δ 194.6 (C = S), 165. (d, $J_{C\text{-}F}$ = 225 Hz), 149.2 (d, $J_{C\text{-}F}$ = 3 Hz), 126.6 (d, $J_{C\text{-}F}$ = 9 Hz), 117.15 (d, $J_{C\text{-}F}$ = 22 Hz), 48.6, 46.0, 14.6, 12.2. FTIR (cm^{-1}): 2984, 1500, 1422,1220,1140,1078,706. Elemental Analysis: (calculated) C_{11} $H_{14}FN_3S$ (239.09) C, 55.21; H 5.90; N, 17.56; (Found) C, 55.21; H, 5.90; N, 17.56; mp: 82 °C.

***N,N*-diethyl-2-(4-(trifluoromethyl)phenyl)diazothioformamide (5d)**: 75 mL of ethanol was degassed under nitrogen flow in a flame-dried round bottom fitted with a magnetic stirrer for 1 h in which *p*-(trifluoromethyl)-phenylhydrazine•HCl (4.25 g, 19.2 mmol) was added and stirred for 0.5 h. Carbon disulphide (1.32 mL, 21.88 mmol) was added dropwise and the solution stirred for 0.5 h. Potassium hydroxide (1.29 g, 232.01 mmol) dissolved in degassed ethanol (25 mL) was then added dropwise in one portion aliquot and the solution stirred for 0.5 h before the addition of methyl iodide (1.33 mL, 21.48 mmol). The solution was stirred for an additional 1 h before concentrating with a rotary evaporator. The flask was then fitted with a reflux condenser and put under nitrogen flow. Diethylamine (40 mL) was added and the solution was refluxed for 48 h. The resulting dark red solution was then allowed to cool before being open to the air and stirred for an additional 2 h. The solution was then washed with brine and extracted with ethyl acetate to afford a dark red liquid. The resulting oil from rotary evaporation was purified using flash column chromatography 7:3 hexane: ethyl acetate yielding 0.71 g (13%) of red solid. The solid was recrystallised via slow evaporation with tetrahydrofuran (THF) to form

diffracting crystals. ^{1}H NMR (300 MHz, Chloroform-*d*) δ 7.97 (d, *J* = 8.3 Hz, 2 H), 7.79 (d, *J* = 8.4 Hz, 2 H), 4.03 (q, *J* = 7.3 Hz, 2H), 3.50 (q, *J* = 7.2 Hz, 2H), 1.42 (t, *J* = 7.1 Hz, 3 H), 1.19 (t, *J* = 7.0 Hz, 3 H). ^{13} C NMR (126 MHz, $CDCl_3$) δ 193.5 (C = S), 153.7, 133.8 (q, $J_{C\text{-}F}$ = 33 Hz), 126.7 (q, $J_{C\text{-}F}$ = 3.8 Hz), 123.81, 123.7 (q, $J_{C\text{-}F}$ = 273 Hz), 48.6, 46.0, 14.5, 12.2. FTIR (cm^{-1}): 2982, 1581, 1434, 1316, 1159, 1079, 773. Elemental Analysis; $C_{12}H_{14}F_3N_3S$ (289.32) (Calculated) C, 49.86; H, 4.96; N, 14.39; (Found) C, 49.82; H, 4.88; N, 14.52; mp: 93 °C.

Determination of pure species molar extinction coefficients

Before binding studies, all ligands and guests were diluted in triplicate to obtain molar extinction coefficients of the pure species. Dilution curves were produced by preparing a stock solution of ATF (or substituted ATF) dissolved in HPLC grade acetonitrile to 0.1125 mM. Starting with pure species at this stock concentration, the absorbance spectra were measured using a ThermoFisher GENESYS 60S UV-Vis Spectrophotometer or a Thermo Scientific Evolution UV-Vis Spectrophotometer. Dilutions were performed in succession by adding 40 µL aliquots of acetonitrile to 1.2 mL of stock ATF using a micropipette, gently mixing, and measuring the absorbance spectra after each aliquot addition, this was repeated 30 times until a final volume of 2.0 mL was achieved. The same dilution procedure described was performed for all ligands and Cu(I) salts, Cu(I)Br, Cu(I)I, and $(CH_3CN)_4Cu(I)BF_4$, dissolved in acetonitrile. Molar extinction coefficients were evaluated from linear absorbance regions which observed Beer–Lambert behaviour.

Determination of H:G binding constants and molar extinction coefficients

UV-Vis spectroscopic titration studies of ATF ligands **1, 5a-d**, and Cu(I) salts were prepared as follows: ligand solutions were prepared to 1.45×10^{-4} M in acetonitrile. A 1.2 mL of ATF solution was added to a quartz cuvette for spectroscopic evaluation. Titrations were performed with Cu(I) halide salts utilising 1.35 mM stock solutions in acetonitrile and sequentially adding 13 µL (roughly 0.1 equivalent of guest) until reaching a guest concentration of three equivalents (a final volume of 2.0 mL). $(CH_3CN)_4Cu(I)BF_4$ salt titrations were performed in the same manner as above to final 1.5 equivalents. Each titration was performed in triplicate. Following data acquisition, the average of each ligand and copper salt spectra was evaluated using non-complexing absorbance models to evaluate wavelength regions where complexation may occur. Additionally, the first-derivative averaged absorbance spectra of ATF ligands **1, 5a-5d** with each copper salt were summed over concentration at each wavelength to identify regions of common maxima (or minima) and compared to absorbance spectra and mixing models to select wavelengths for calculating binding association constant information. First derivative analysis showed maxima with all copper salts for a specific ATF ligand **1, 5a-c** at wavelengths of 348, 414, 367, 352 nm, respectively. First derivative analysis for ligand **5d** gave an inflection point at a non-zero value of 324 nm, and this was used for further analyses (see Figure S14). For each replicate, absorbance values from four additional wavelengths (−4, −2, +2, +4 nm of maxima) were used to predict binding behaviour for ATF ligands **1, 5a-d**. Binding association constants were calculated utilising non-linear binding regression models for 1:1 and 2:1 statistical, full, additive, and non-cooperative models in Bindfit [9,10].

Computational studies

All structures were fully optimised without symmetry constraints using the B3LYP functional as implemented in Gaussian 09 using the 6–31 G** basis set for C, H, N, S, Br, B, F, and P and the Stuttgart basis set with effective core potentials for all metal and iodine atoms. To verify the validity of the chosen method, other DFT functionals were used: B3LYP-D3, B3P86, B3PW91, M11, and wB97XD, but B3LYP gave structural parameters that best matched the experimental structures. The ultrafine integration grid was employed in all calculations, which ensured the stability of the optimisation procedure for the investigated molecules. Each stationary point was confirmed by a frequency calculation at the same level of theory to be a real local minimum on the potential energy surface. More accurate electronic energies were computed for the optimised geometries using the larger 6–311++G(d, p) basis set. All reported free energies are for tetrahydrofuran solution at the standard state (T = 298.15 K, P = 1 atm, 1 mol/L concentration of all species in THF) as modelled by a polarised continuum model. The energy values given in the manuscript correspond to solvent-corrected Gibbs free energies that are based on B3LYP/6-311++G(d,p) electronic energies and all corrections calculated at the B3LYP/6-31 G(d) level.

Results

Synthesis and X-ray crystal structures

Substituted ATF ligands were synthesised based on various electron-donating or electron-withdrawing groups following known one-pot procedures [4,6]. Preparation was straightforward from commercially available phenylhydrazine HCl salts (**4a-d**) as shown in Scheme 2. Ligand yields varied with all but the strongly electron-withdrawing CF_3 substituted

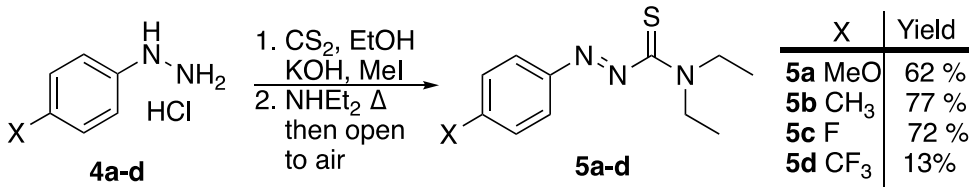

Scheme 2. One Pot Synthesis of variably substituted ATF ligands 5a-d.

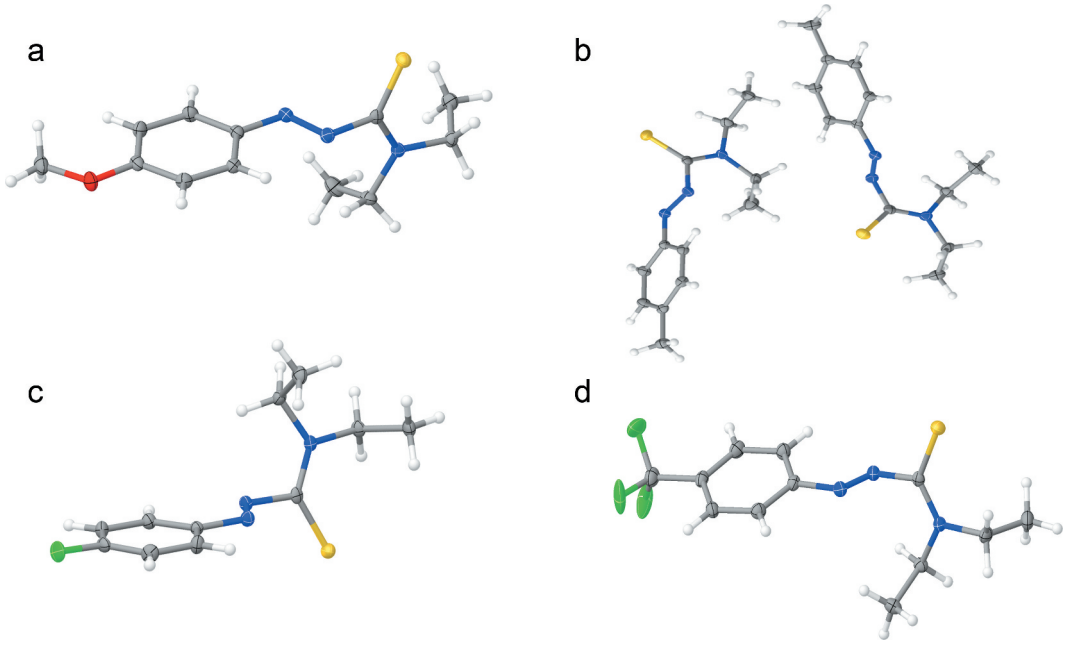

Figure 1. Asymmetric units of X-ray crystal structures for ligands **5a-d**. A) ligand **5a**; B) **5b** where the asymmetric unit displayed two similar but unique structures; C) **5c;** D) **5d**.

Table 1. Bond distances and angles for 1,4-heterodiene units of substituted ATF ligands from single-crystal x-ray diffraction.

	Bond distances from XRD data (in Å)			Bond angles from XRD		
Ligand	N=N	N-C	C=S	S1-C1-N1	C1-N1-N2	N1-N2-C2
5a MeO-ATF	1.257(7)	1.435(8)	1.670(6)	117.74	113.89	114.72
5b Me-ATF†	1.252(4)	1.440(1)	1.663(3)	118.28	112.40	114.07
	1.250(9)	1.435(9)	1.665(0)	119.20	112.77	114.52
1 ATF*	1.244(0)	1.440(0)	1.662(0)	117.8	114.3	114.42
5 c F-ATF	1.252(0)	1.435(8)	1.667(4)	118.09	114.36	114.15
5d CF_3-ATF	1.254(0)	1.445(0)	1.663(0)	116.43	110.81	114.54

*These values were obtained from previous report[6].
†Note that the Z′ for this crystal is 2 and two independent but similar structures were found in the asymmetric unit cell.

ligand (**5d**) providing a modest one-pot yield. Attempts to isolate the xanthate ester intermediate to optimise the reaction for **5d** only sparingly increased the yield. All ligands were purified through column chromatography and recrystallised through evaporative concentration from tetrahydrofuran or acetonitrile yielding diffracting crystals of X-ray quality as shown in Figure 1.

Table 1 provides bond lengths and torsional angles of the 1,4- azothiocarbonyl heterodiene units of the synthesised and recrystallised ligands **5a-d**. Comparisons of bond distances for the N=N, N-C, and C=S and bond angles of the heterodiene from the previously reported ATF crystal structure of **1** show very little difference and indicate that the substituents on the phenyl ring have little influence on the asymmetric unit ligand structure before coordination. As seen above in Figure 1, MeO-ATF derivative, **5a**, when in crystalline form, displays both of its ethyl groups in the same direction instead of the lower energy staggered conformation. This same phenomenon was seen when non-substituted **1** was crystallised with silver(I) and dense crystal packing was argued to induce this higher energy state[11]. Full crystallisation parameters and tables can be found in supporting information (ESI).

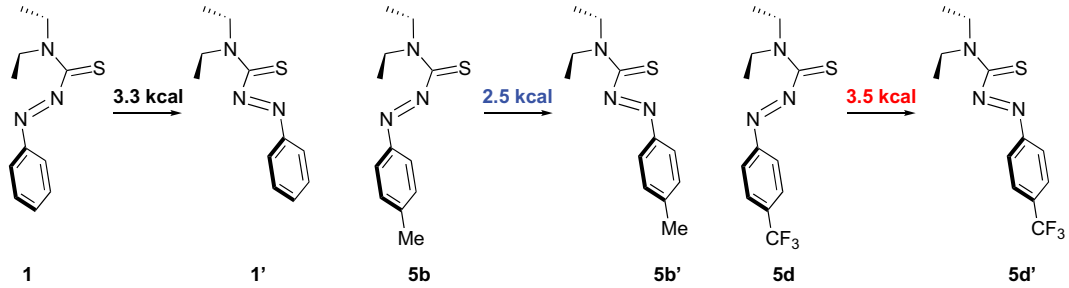

Scheme 3. Representative example of the calculated energy of rotation for the crystalline ligands.

Computational modelling

For association to occur, the ligands must rotate from their lowest energy *s*-trans crystalline state into an *s*-cis 1,4-azothiocarbonyl configuration. In the previous report, non-substituted ATF ligand **1** was modelled to require 3.3 kcal/mol to attain a binding configuration in a neutral transition state. The rotational energy barriers of the para-substituted ATF analogues **5a-d** as neutral transition states were modelled and these values are shown in **Table S2**. As predicted, the electron-donating substituted ligands **5a** and **5b** require less energy for rotation compared with unsubstituted and the strong electron-withdrawing CF_3 substituted ligand **5d** has a predicted larger energy of rotation than non-substituted. This rotation is illustrated in Scheme 3 with representative examples of **1, 5b**, and **5d** rotating into coordination as **1', 5b'**, and **5d'** respectively. Interestingly, computational predictions suggested that *p*-fluoro substituted derivative **5c** to be similar to the unsubstituted ligand **1** and perhaps the small size of the fluorine atom and the slightly donating resonance contribution of the halogen provides this slight decrease in energy to overcome the rotational barrier.

Following the rotational energy models, metal to ligand associations were modelled utilising a 6–311 G+ +G(d,p) basis set as to obtain free energies and subsequently calculate equilibrium constants to compare these values with those found with titration experiments. Shown in Scheme 4 is a representative example for the variant ATF ligands, shown is ligand **5c** associating to a Cu(I)Br and Cu(I)I with loss of an acetonitrile in a 1:1 coordination yielding structure **6** and **7** respectively, and **5c** undergoing both 1:1 coordination to give **8** while continuing in the two-step model for 2:1 coordination and predicted structure **9** (Full binding diagrams can be found in the supporting information Figures S2-S6). Table 2 displays the binding energies and calculated K values for these coordination complexes to both 1:1

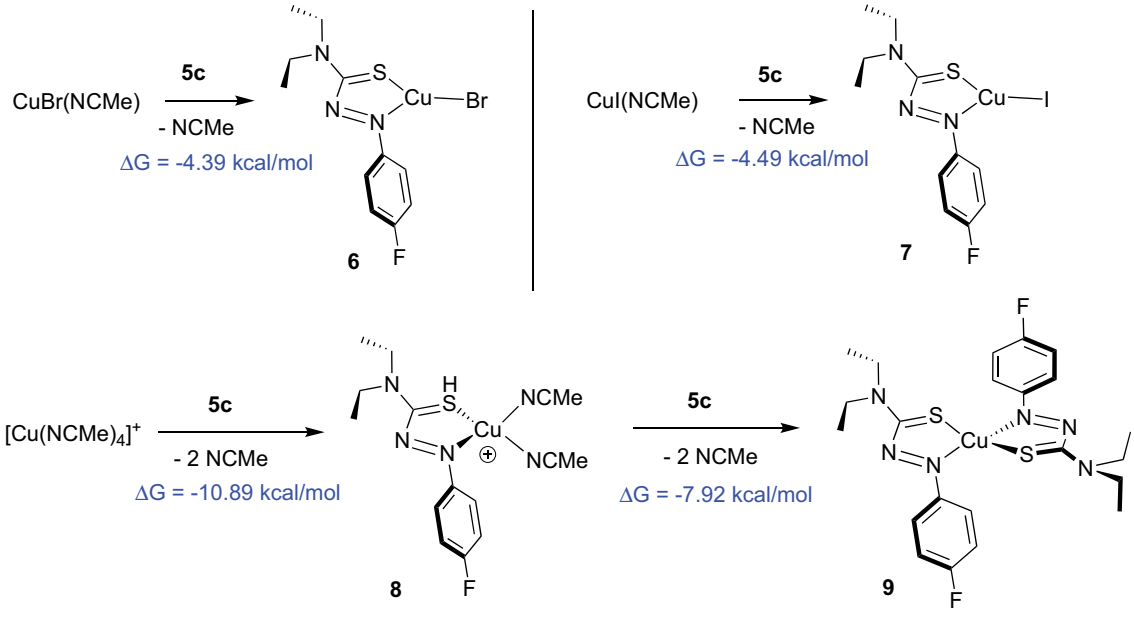

Scheme 4. Representative example of ligand 5c when bound to the various Cu(I) salts.

Table 2. Gibb's energy, association constant, and substituent ratio from DFT modelling.

	CuBr			CuI		
Sub.	**ΔG (kcal/mol)**	**K_{a1}**	**K_{a1i}/K_{aATF}**	**ΔG (kcal/mol)**	**K_{a1}**	**K_{a1i}/K_{aATF}**
ATF	−4.5	2.00E+03	1.0	−4.6	2.36E+03	1.0
MeO	−6.82	1.00E+05	50.0	−6.9	1.15E+05	48.7
Me	−5.47	1.03E+04	5.2	−5.57	1.22E+04	5.2
F	−4.39	1.66E+03	0.8	−4.49	1.96E+03	0.8
CF_3	−3.59	4.29E+02	0.2	−3.64	4.67E+02	0.2
	$(CH_3CN)_4CuBF_4$ (addition of first ligand)			**$(CH_3CN)_4CuBF_4$ (addition of second ligand)**		
Sub.	**ΔG (kcal/mol)**	**K_{a1}**	**K_{a1i}/K_{aATF}**	**ΔG (kcal/mol)**	**K_{a2}**	**K_{ai}/K_{a2ATF}**
ATF	−10.7	7.04E+07	1.0	−8.2	1.03E+06	1.0
MeO	−12.52	1.52E+09	21.6	−10.87	9.38E+07	91.1
Me	−11.38	2.22E+08	3.2	−10.32	3.71E+07	36.0
F	−10.89	9.70E+07	1.4	−7.92	6.44E+05	0.6
CF_3	−10.14	2.73E+07	0.4	−6.59	6.81E+04	0.1

and predicted 2:1 coordination complex. For the 1:1 cases there were two obvious trends for the association constants: 1) that stronger electron-donating substituents (**5a, 5b**) released more exothermic energy upon complexation and thus larger equilibrium constants and stronger associations than non-substituted **1** and electron-withdrawing substituted ATFs (**5c, 5d**); 2) when comparing Cu(I)Br and Cu(I)I, the less electronegative and larger iodide atom was slightly more exothermic and therefore increased the binding association constants of these salts. For the predicted 2:1 association, the binding energy for the first ligand addition can be modelled separately from the second ligand association. Expectedly, the first association was multiple orders of magnitude larger in energy than the second but both being more appreciable than a predicted 1:1 interaction providing ample delivery of a 2:1 coordination complex as a favourable interaction. Again, when comparing **5a-d**, the trend of electron-donating groups increasing the association constant was observed with the **5a** being the strongest and CF_3 substituent **5d** being predicted to be the weakest bound neutral species.

From the energies associated with predicted 1:1 binding, equilibrium constants were calculated as potential guidelines for experimental data. Table 2 displays the equilibrium constants (K_{eq}) for the various ligands when coordinated.

Binding coordination studies

Supramolecular binding association constants are the most commonly included calculable feature when reporting H:G interactions [12,13]. Non-linear association models (isotherms) have seen increased use in recent years over the classic linear regression methods (i.e. Benesi-Hildebrand) [14,15]. All pure species of ligands show a high degree of linearity near the 200–500 nm range as seen in Figure 2 with coefficient of determination (R^2) greater than 0.99. Ligand hosts show virtually no signal in the latter portions of the visible spectrum, even at elevated concentrations.

Figure 3 illustrates absorbance spectra of ATF ligands **1, 5a-d** when titrated with Cu(I)Br (similar spectra of Cu(I)I and $(CH_3CN)_4Cu(I)BF_4$ salt titrations are shown in Figure S12-S13). Titration studies resulted in the formation of observable shifts in the absorbance spectra that differ from the pure ligand absorbance spectra and most likely indicate an ATF-Cu complex. Ligands with more electron-donating groups (**5a-b**) show pronounced peak shifts in the 250–400 nm range towards lower energy in the 300–500 nm wavelengths. Ligand **1** and **5c**, present very similar spectra. Ligand **5d** shows the least pronounced absorbance response to increasing Cu(I) salt concentrations and the lowest molar extinction coefficients of **1, 5a-d** ligands evaluated.

Shown in Figure 4 are isotherms associated with Cu(I) bromide and the ligand library. The compiled isotherms indicate that the electron-donating substituents, ligands **5a-b**, result in a higher binding association constant compared to non-substituted ligand **1** or electron-withdrawing substituted (ATF ligands **5c-d)** and was observed in Cu(I)I and $(CH_3CN)_4Cu(I)BF_4$ (additional isotherms can be found in ESI Figures S15-16). Bindfit values for 2:1 H:G coordination are presented in Table 3.

Discussion

Electron-donating species produced higher molar extinction coefficients compared to electron-withdrawing groups in the order **5a**>**5b**>**1**≈**5c**>**5d** (see Figure 4). This relationship was observed regardless of guest species introduced. Through X-ray diffraction of ligand **1, 5a-d** crystals, no substantial variance in bond distance and bond angles was observed, suggesting differences in binding with guests are driven by electronic interaction from substituents. Table 2 shows a similar trend in the predicted H:G DFT models.

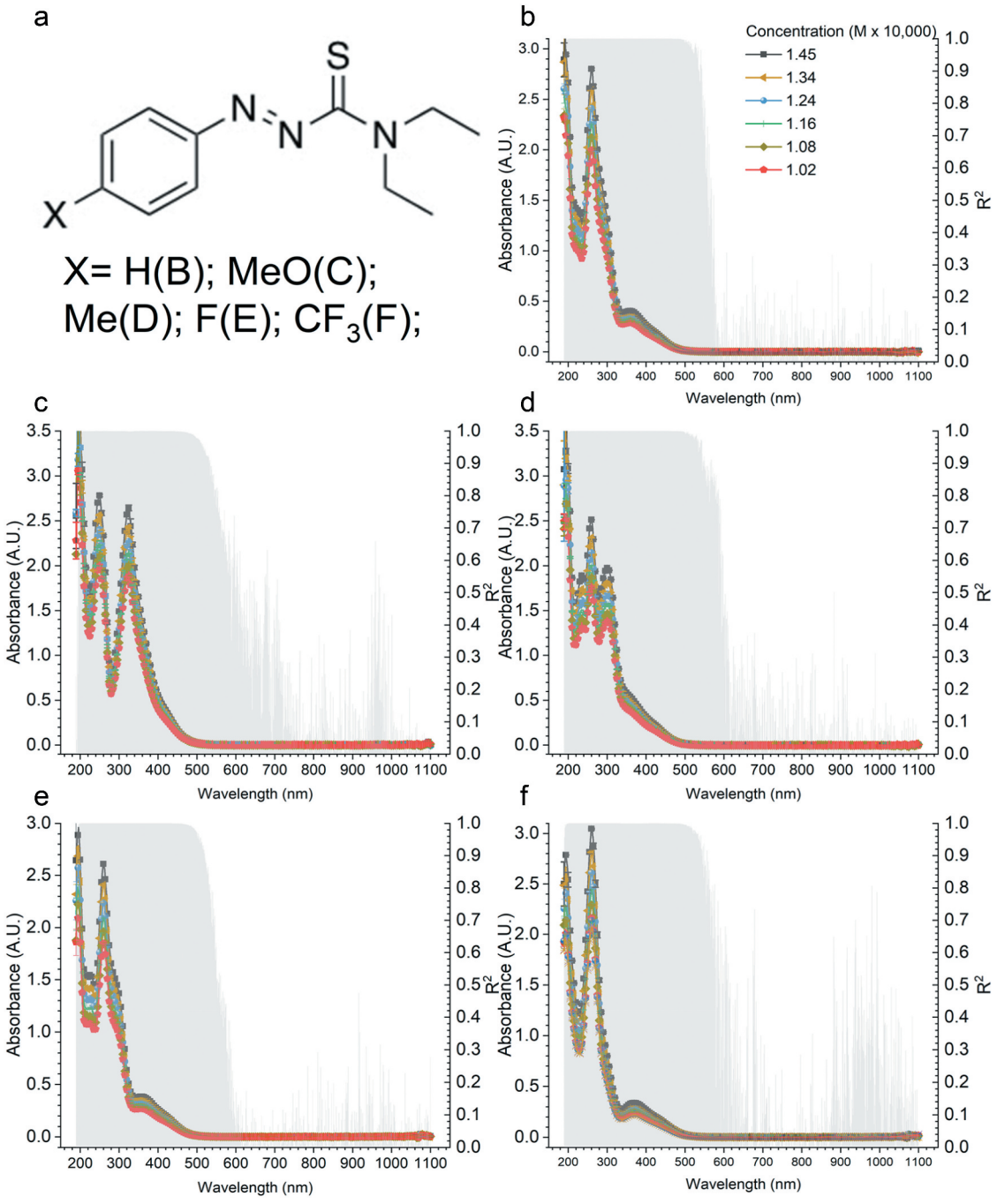

Figure 2. UV-visible absorbance spectra (left axes) and coefficient of determination (R^2) (right axes) of ATF ligands **1, 5a-d**. For clarity, only every 5th data point from dilution curves are shown. Error bars are the standard error between replicate samples.

Copper halides with ligands were expected to fit a 1:1 model based on DFT from Johnson et al. [6], because the addition of another host was predicted to result in a positive ΔG for 2:1 and 2:2 μ-X dimers and as a 2:1 H:G for $(CH_3CN)_4Cu(I)BF_4$ complexes of ATF ligand **1, 5a-d**. In all cases using Bindfit to predict interactions, 1:1 models were a poor fit (data not shown). Full, additive, non-cooperative, and statistical 2:1 H:G models were evaluated against spectroscopic data for copper halide and BF_4 species (shown in Table 3); each model fits reasonably well, though some results were likely non-physical.

Non-coordinative $(CH_3CN)_4Cu(I)BF_4$ species show equivalent absorbance values for spectra compared to halides at half the equivalent concentration, suggesting a 2:1 additive or statistical model from spectroscopic

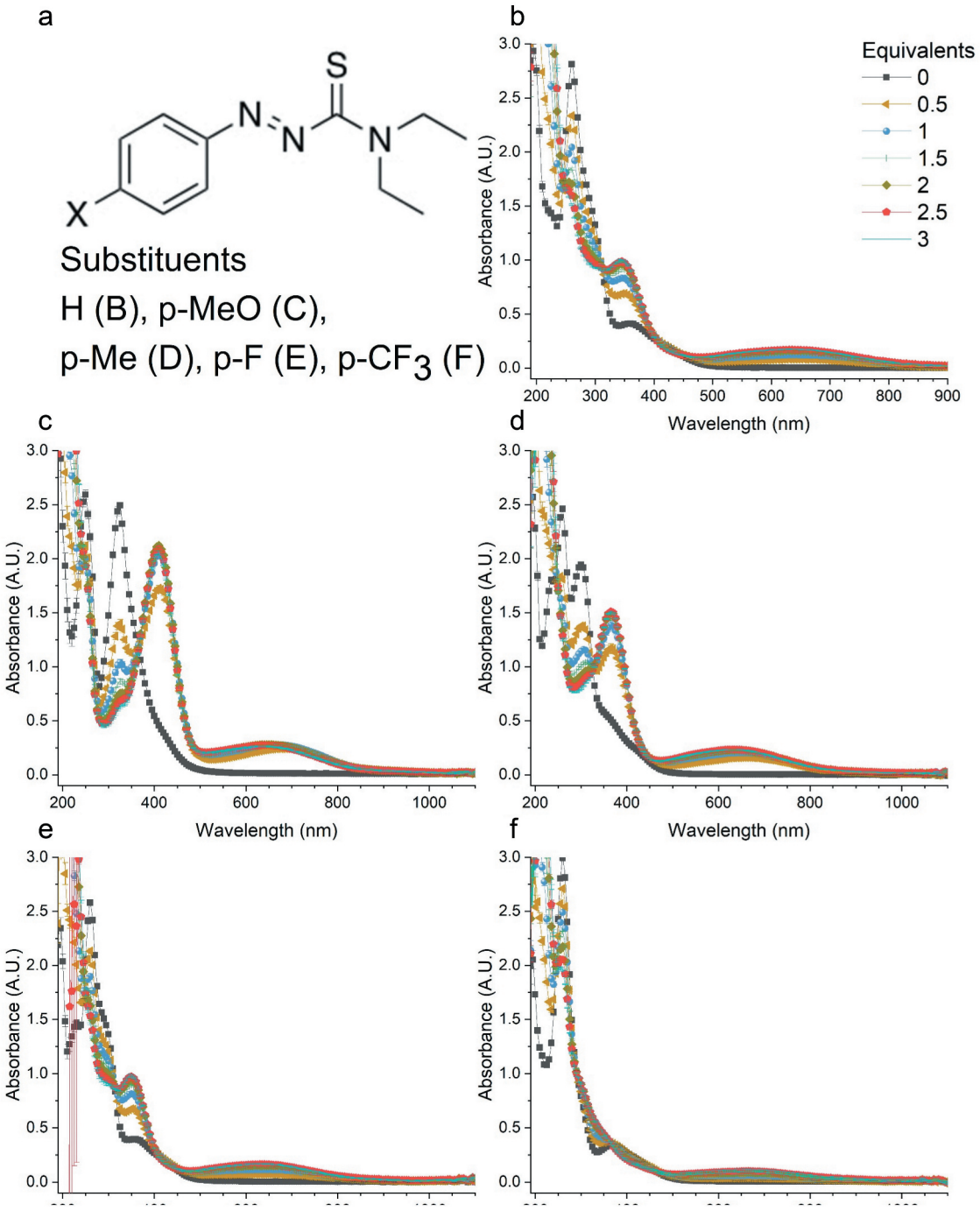

Figure 3. UV-visible spectra of Cu(I)Br titrations with ATF ligands **1, 5a-d**. For clarity, only every 5th data point from titration curves are shown. Error bars are the standard error between triplicate samples.

observations. DFT modelling predicted that a 'full' model, in addition to additive or statistical, could describe binding of host with $(CH_3CN)_4Cu(I)BF_4$ as the H:G complex with its non-coordinating counter ion was able to accept a second host with a predicted negative ΔG. For $(CH_3CN)_4Cu(I)BF_4$ complexes, full or additive models ranked more favourably using Bayesian-Information-Criterion (BIC) though this trend decreased with increasing electron-donating substitution towards full or non-cooperative models. While still predicted to be 2:1 in nature, $(CH_3CN)_4Cu(I)BF_4$ complexes with electron-withdrawing substituents favour asymmetric (full, additive) models while more electron-donating substituents favour more symmetric (non-cooperative, statistical) models and this symmetry is supported by DFT predictions (Figures S2-6). The hypothesis that electronic structure influences binding strength, with more electron-withdrawing groups showing weaker binding while

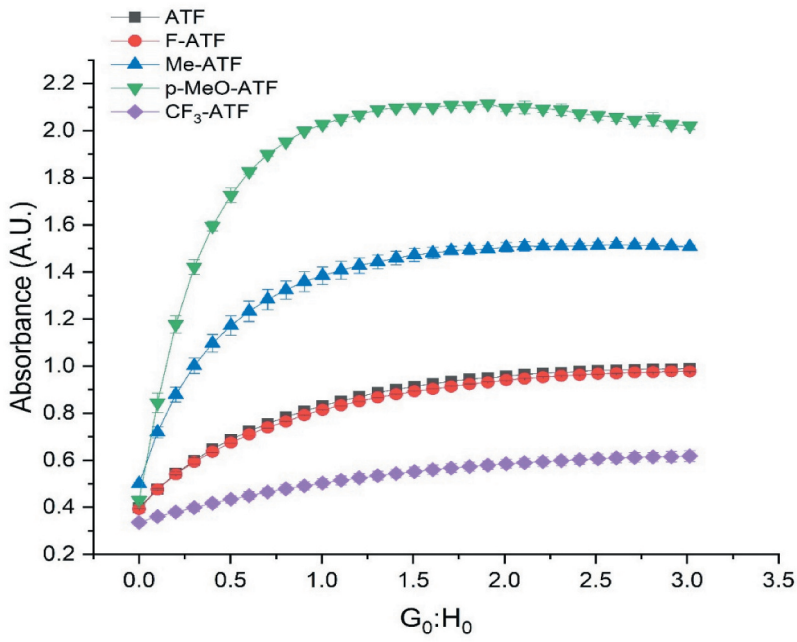

Figure 4. Binding isotherms of ligands **1, 5a-d**, at comparable wavelengths for the titration of Cu(I)Br. Error bars are the standard error between triplicate samples.

electron-donating groups show stronger binding, was supported in full, additive, and statistical models for K_{A1}, shown in the Hammett plot (Figure 5) and some K_{A2} models (ESI Fig. S19). As association constants, K_{A1} and K_{A2}, for both non-cooperative and statistical models are related by a scalar of 4, if K_{A1} was significant for these models, K_{A2} showed identical results. Each of these models showed significantly different slopes from zero (p-value < 0.03) and were of high correlation (adjusted $R^2 > 0.77$). DFT models for $(CH_3CN)_4Cu(I)BF_4$ complexes with **1, 5a-d** displayed similar correlations (adj. $R^2 \approx 0.69$) but were not significant at the 0.05 level (p-value of 0.052).

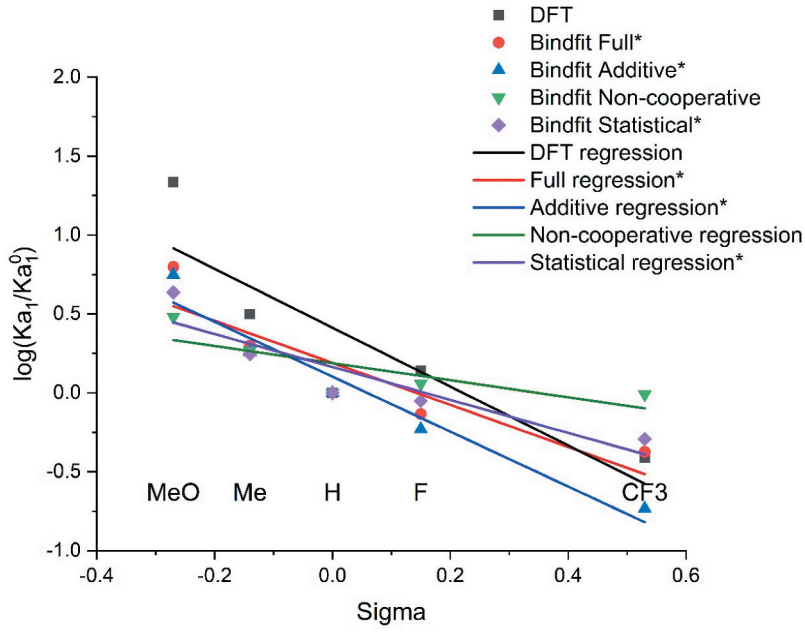

Figure 5. Hammett plot of ATF ligands 1, 5a-d for $(CH_3CN)_4Cu(I)BF_4$ complexes. Each substituent was normalised to ATF ligand 1 (Ka_1^0). All models show similar trend of increasingly electron-donating substituents showing increased binding affinity. Slopes for models with an asterisk are significantly different than zero at a 0.05 level.

Table 3. 2:1 H:G models fit of CuBr, CuI, and $(CH_3CN)_4CuBF_4$ with ATF ligands 1, 5a-d using Bindfit.

Guest	Host	K_{A1} ± % K_{A1}		K_{A2} ± % K_{A2}		RMS	Cov ratio	SSR	BIC
CuBr	***Full***								
	CF_3-ATF	1,525	± 0.9916	1.53E-06	± 0.5912	1.25E-03	0.29	4.35E-04	718.75
	F-ATF	6,172	± 2.8801	1,961	± 3.2027	3.13E-03	0.78	4.55E-03	481.89
	ATF	1,224	± 0.7002	6,075	± 0.3840	2.57E-03	0.28	3.08E-03	521.37
	Me-ATF	2,386	± 0.8028	26,295	± 0.3826	4.72E-03	0.15	1.04E-02	398.67
	MeO-ATF	4,724	± 0.8361	27,113	± 0.2503	9.81E-03	0.24	4.48E-02	251.01
	Additive								
	CF_3-ATF	35,151	± 2.3478	737	± 3.0097	1.72E-03	0.55	8.29E-04	673.75
	F-ATF	6,064	± 10.2267	2,104	± 11.4615	3.51E-03	0.99	5.73E-03	478.47
	ATF	13,279	± 3.3472	1,078	± 5.1132	4.76E-03	0.95	1.05E-02	417.14
	Me-ATF	5,360	± 2.9528	14,940	± 1.5508	1.03E-02	0.73	4.93E-02	261.33
	MeO-ATF	14,994	± 2.4613	17,569	± 0.7819	1.67E-02	0.70	1.29E-01	164.19
	Non-cooperative								
	CF_3-ATF	1,475	± 0.0567	369	-	1.30E-03	0.31	4.71E-04	712.10
	F-ATF	6,610	± 0.1542	1,653	-	3.13E-03	0.79	4.57E-03	482.75
	ATF	3,400	± 0.0777	850	-	2.86E-03	0.34	3.79E-03	501.50
	Me-ATF	15,479	± 0.3012	3,870	-	8.55E-03	0.50	3.40E-02	280.09
	MeO-ATF	20,441	± 0.3516	5,110	-	1.68E-02	0.71	1.31E-01	143.81
	Statistical								
	CF_3-ATF	7,259	± 0.2513	1,815	-	2.33E-03	1.00	1.52E-03	613.88
	F-ATF	7,105	± 0.1807	1,776	-	3.53E-03	1.00	5.80E-03	478.68
	ATF	7,639	± 0.2386	1,910	-	4.88E-03	1.00	1.11E-02	413.49
	Me-ATF	16,177	± 0.4329	4,044	-	1.21E-02	1.00	6.76E-02	230.69
	MeO-ATF	30,735	± 0.5608	7,684	-	1.99E-02	1.00	1.84E-01	129.80
CuI	***Full***								
	CF_3-ATF	2,775	± 1.6250	3.80E-07	± 0.9934	6.79E-03	0.47	1.29E-02	376.90
	F-ATF	1,320	± 0.5462	1,843	± 0.267	2.35E-03	0.18	2.57E-03	539.58
	ATF	1,383	± 0.5410	6,303	± 0.2807	2.61E-03	0.20	3.17E-03	518.28
	Me-ATF	2,584	± 0.5287	10,440	± 0.1974	4.11E-03	0.15	7.85E-03	426.77
	MeO-ATF	13,127	± 0.9403	7,552	± 0.2332	1.22E-02	0.19	6.87E-02	207.72
	Additive								
	CF_3-ATF	75,684	± 9.1424	761	± 9.4111	8.86E-03	0.13	2.19E-02	343.10
	F-ATF	20,333	± 1.6901	494	± 4.9552	4.23E-02	6.95	8.33E-03	440.78
	ATF	15,840	± 3.1540	1,230	± 4.3587	5.55E-03	0.81	1.43E-02	386.19
	Me-ATF	9,573	± 3.5462	6,552	± 1.7957	1.00E-02	0.48	4.69E-02	266.21
	MeO-ATF	30,542	± 4.0668	12,614	± 1.0236	2.71E-02	0.48	3.43E-01	65.45
	Non-cooperative								
	CF_3-ATF	2,649	± 0.2803	662	-	6.94E-03	0.50	1.35E-02	373.72
	F-ATF	1,862	± 4.3824e-2	466	-	2.44E-03	0.19	2.77E-03	533.20
	ATF	3,873	± 0.0657	968	-	2.96E-03	0.26	4.08E-03	494.25
	Me-ATF	8,005	± 0.1352	2,001	-	6.32E-03	0.36	1.86E-02	341.13
	MeO-ATF	17,817	± 0.2093	4,454	-	1.27E-02	0.21	7.55E-02	199.53
	Statistical								
	CF_3-ATF	8,037	± 0.8082	2,009	-	9.86E-03	1.00	2.71E-02	322.96
	F-ATF	7,104	± 0.2567	1,776	-	5.61E-03	1.00	1.46E-02	385.35
	ATF	8,740	± 0.2333	2,185	-	5.80E-03	1.00	1.56E-02	378.62
	Me-ATF	15,934	± 0.3738	3,984	-	1.05E-02	1.00	5.11E-02	258.95
	MeO-ATF	39,504	± 0.8176	9,876	-	2.76E-02	1.00	3.53E-01	63.74
$(CH_3CN)_4CuBF_4$	***Full***								
	CF_3-ATF	814	± 4.0641	42,849	± 2.9122	1.48E-03	0.81	6.12E-04	684.31
	F-ATF	1,416	± 1.0626	14,895	± 0.6924	1.30E-03	0.38	7.91E-04	658.48
	ATF	1,926	± 1.7418	8,724	± 1.0016	3.23E-03	0.70	4.69E-03	478.67
	Me-ATF	3,851	± 0.6787	10,853	± 0.2868	2.72E-03	0.23	3.44E-03	510.08
	MeO-ATF	12,099	± 2.3260	19,799	± 0.5936	1.89E-02	0.35	1.57E-01	124.08
	Additive								
	CF_3-ATF	1,055	± 10.9097	25,633	± 7.2082	1.60E-03	0.95	7.16E-04	688.57
	F-ATF	3,372	± 4.2548	9,883	± 3.2144	1.78E-03	0.71	1.47E-03	615.91
	ATF	5,710	± 8.9435	6,810	± 6.4410	3.68E-03	0.90	6.09E-03	472.40
	Me-ATF	10,337	± 3.1608	12,487	± 1.5671	4.65E-03	0.68	1.00E-02	421.90
	MeO-ATF	31,974	± 7.9417	28,292	± 1.9562	2.97E-02	0.91	4.11E-01	47.03
	Non-cooperative								
	CF_3-ATF	6,620	± 0.6060	1,655	-	1.56E-03	0.89	6.76E-04	675.75
	F-ATF	7,731	± 0.0942	1,933	-	1.75E-03	0.68	1.42E-03	600.94
	ATF	6,764	± 0.1264	1,691	-	3.49E-03	0.81	5.47E-03	464.63
	Me-ATF	12,496	± 0.0978	3,124	-	3.88E-03	0.47	7.00E-03	439.63
	MeO-ATF	20,483	± 0.3363	5,121	-	2.20E-02	0.50	2.26E-01	89.00
	Statistical								
	CF_3-ATF	6,739	± 0.6404	1,685	-	1.65E-03	1.00	7.56E-04	684.34
	F-ATF	11,742	± 0.1496	2,935	-	2.11E-03	1.00	2.07E-03	582.75
	ATF	13,216	± 0.2197	3,304	-	3.87E-03	1.00	6.74E-03	463.53
	Me-ATF	23,330	± 0.2202	5,833	-	5.64E-03	1.00	1.48E-02	383.99
	MeO-ATF	57,224	± 1.0159	14,306	-	3.11E-02	1.00	4.51E-01	39.13

RMS: root mean squared error; cov ratio: covariance ratio; SSR: sum of square residuals; BIC: Bayesian Information Criterion; $K_{A1} = 4{\cdot}K_{A2}$ for non-cooperative and statistical models, so error reported for K_{A1} is identical to K_{A2} for these models.

Copper halide data fit reasonably well with different 2:1 models but did not show the same features as $(CH_3CN)_4Cu(I)BF_4$ complexes. BIC for full (asymmetric) or non-cooperative (symmetric) models was ranked identically with both halide species. Non-cooperative and statistical models match the closest to our substituent hypothesis pattern with electron-withdrawing groups showing weaker coordination than electron-donating groups. The ambiguity of the asymmetric and symmetric predictions may suggest that a different binding mechanism may be occurring. Regression models of Hammett plots for Cu(I)Br complexes (ESI Fig. S17) showed DFT and non-cooperative models as significantly different than zero (p-value <0.035), while only DFT models were significantly different than zero (p-value ≈ 0.031) for Cu(I)I complexes (ESI Fig. S18), though trends followed the substituent hypothesis (except additive with CuI).

By synthesising and investigating a small library of substituted redox-active ATF ligands it was found that electron-donating moieties resulted in more exothermic interactions, larger extinction coefficients, and an increased predicted binding association. Electron-withdrawing moieties provided weaker binding association interactions and no evidence of a reduction event as indicated by spectral shift. Computational predicted association values followed similar trends with a relative strength of coordination is of the order MeO-ATF > Me-ATF > ATF ≈ F-ATF > CF_3-ATF for para-substituted species.

Overall, computational models and crystal structures of ligands can provide valuable predictive information for experimental studies, even if absolute values disagree. Understanding H:G interactions with metal centres contributes to both catalyst design, organic synthesis, and quantitative analysis. A better understanding of how substitution impacts binding will allow for future refinements in computational tools for predicting binding interactions.

acknowledgement:

X-ray crystallographic data were collected at the University of Montana X-ray diffraction core facility supported by the Center for Biomolecular Structure and Dynamics CoBRE (National Institutes of Health, CoBRE NIGMS P20GM103546). Single crystal X-ray diffraction data were collected using a Bruker D8 Venture, principally supported by [NSF MRI CHE-1337908].

Disclosure statement

The authors declare no financial interests.

Funding

The M.J. Murdock Charitable Trust, Vancouver, WA, Reference No.: 2014120: 11/20/2014, provided funds supporting the purchase of a 500 MHz NMR spectrometer. Computational resources for DFT calculations were provided by Washington State University.

ORCID

James G. Moberly http://orcid.org/0000-0003-0950-0952
Kristopher V. Waynant http://orcid.org/0000-0002-4096-5726

References

[1] Bechgaard K. Nonplanar electron-transfer complexes .2. chemistry of 4 Cu-N2s2z complexes derived from copper-Bis-N,N-diethylphenylazothioformamide. Acta Chem Scand A. **1977**;31(8):683–688. .
[2] Bechgaard K. Nonplanar electron-transfer complexes .1. Chemistry of 5 Ni-N2s2z complexes derived from nickel-Bis-N,N-diethylphenylazothioformamide. Acta Chem Scand A. **1974**;A 28(2):185–193. .
[3] Nielsen KT, Bechgaard K, Krebs FC. Removal of palladium nanoparticles from polymer materials. Macromolecules. **2005**;38(3):658–659.
[4] Nielsen KT, Bechgaard K, Krebs FC. Effective removal and quantitative analysis of Pd, Cu, Ni, and Pt catalysts from small-molecule products. Synthesis-Stuttgart. **2006**;10:1639–1644.
[5] Nielsen KT, Harris P, Bechgaard K, et al. Structural study of four complexes of the M-N2S2 type derived from diethylphenylazothioformamide and the metals palladium, platinum, copper and nickel. Acta Crystallogr B. **2007**;63(Pt 1):151–156.
[6] Johnson NA, Wolfe SR, Kabir H, et al. Deconvoluting the innocent vs. non-innocent behavior of N, N-diethylphenylazothioformaide ligands with copper sources. Eur J Inorg Chem. **2017**;47:5576–5581.
[7] Guo J-Y, Minko Y, Santiago CB, et al. Developing comprehensive computational parameter sets to describe the performance of pyridine-oxazoline and related ligands. ACS Catal. **2017**;7(6):4144–4151.
[8] Nielsen KT, Bechgaard K, Krebs FC. Effective removal and quantitative analysis of Pd, Cu, Ni, and Pt catalysts from small-molecule products. Synthesis. **2006**;2006 (10):1639–1644.
[9] Brynn Hibbert D, Thordarson P. The death of the Job plot, transparency, open science and online tools, uncertainty estimation methods and other developments in supramolecular chemistry data analysis. Chem Commun. **2016**;52(87):12792–12805.
[10] Available from: http://supramolecular.org. Accessed June 10th, 2020.
[11] Groner VM, Larson GE, Kan Y, et al. The synthesis and crystal structure of bis-[3,3-diethyl-1-(phenyl-imino-kappaN)thiourea-kappaS]silver hexa-fluorido-phosphate. Acta Crystall ogr E Crystallogr Commun. **2019**;75(Pt 9):1394–1398.

[12] Steed JW, Atwood JL. Supramolecular chemistry. 2nd ed. Chichester, UK: Wiley; 2009. p xxvi, 970 p., 8 p. of plates.
[13] Cragg PJ. Supramolecular chemistry: from biological inspiration to biomedical applications. Supramol Chem. **2010**;1–260.
[14] Hargrove AE, Zhong ZL, Sessler JL, et al. Algorithms for the determination of binding constants and enantiomeric excess in complex host: guest equilibria using optical measurements. New J Chem. **2010**;34 (2):348–354.
[15] Thordarson P. Determining association constants from titration experiments in supramolecular chemistry. Chem Soc Rev. **2011**;40(3):1305–1323.